Giant, 5, 2021, 100041

Mimicking evolution of 'mini-homeostatic' modules in supramolecular systems

Santanu Panja, Dave J. Adams*

School of Chemistry, University of Glasgow, Glasgow G12 8QQ, UK

Natural systems maintain steady internal, physical, and chemical conditions (i.e. they exhibit homeostasis) and keep control over their local environment by creating many mini-homeostatic modules. In comparison, synthetic materials are typically formed under equilibrium or kinetically trapped conditions and do not usually change their properties with time. Hence, synthetic systems are typically devoid of self-regulation, self-correction and self-monitoring. Because of their static nature, reconfiguration of synthetic systems is also difficult as they exhibit unidirectional responses to perturbation. Here, we describe a hydrogel-based homeostatic system with self-monitoring and self-regulating properties over a cyclic energy input. Unlike other dynamic gels under feedback loops, our system maintains its gel form throughout the energy cycle across a wide pH range. Control over the evolution of the mini-homeostatic modules induces a self-correcting property to our homeostatic hydrogel which can tune the network type and improve the mechanical properties of the system.

Natural systems can show self-correcting and self-regulating behaviour as they are controlled by feedback loops. [1–4] Natural processes which exhibit such reversible autonomous regulation typically involve three stages following either an inactive-active-inactive [3–5] or a static-active-static [2, 6] configuration. For example, natural self-assembled systems operate in an inactive-active-inactive fashion where an active assembly state is formed transiently from the non-assembling entities in the presence of an energy source (a fuel). [3–5, 7] The assembled structures persist whilst the energy source is available. Once it runs out, the system reverts to its original, non-assembled state. A typical example is the guanosine-5'-triphosphate (GTP) induced polymerization of tubulin dimers to form microtubules. [8]

Natural processes like control of body temperature, maintenance of heart rate, blood pressure, pH and sugar levels, muscle contraction etc. follow a complex mechanism where the system maintains its integrity over time while constantly interacting with its environment. [2, 6, 9] These are homeostatic systems and the ability to control of their local environment (or sustain their integrity) in response to perturbation is called homeostasis. [2, 6, 9, 10] Homeostasis is a fundamental concept in biology, which refers to the ability of living systems to maintain stability of their internal environment while a breakdown of homeostasis is considered as the hallmark of a disease progression. [11] There is several homeostasis found in biology, for example, Zn^{2+}-homeostasis, [12] Cu^{2+}-homeostasis, [13] urate homeostasis, [14] tensional homeostasis, [11] protein homeostasis [15] etc., by which a living system maintains a fairly constant or steady state when they are affected by conditions tending to perturb them. [16] Systems exhibit homeostasis through interconversion of

* Corresponding author.
E-mail address: dave.adams@glasgow.ac.uk (D.J. Adams).
Received 4 November 2020; Received in revised form 1 December 2020; Accepted 8 December 2020

 https://doi.org/10.1016/j.giant.2020.100041

chemical and mechanical energy under self-regulating feedback loops and create hierarchy across the time scales. [6, 10] Each individual level that is temporally created can be addressed as mini-homeostatic 'modules' which are the inherent core of a homeostatic system. In the presence of a stimulus, a homeostatic system operates through successive combination of mini-homeostatic modules, with some modules responding to a stimulus and others opposing the stimulus to maintain overall homeostasis (static-active-static mode). [6, 10] Hence, paired opposing modules inherently provide self-correcting behaviour to the homeostatic systems.

Supramolecular low molecular weight hydrogels are an important class of soft materials having multifunctional applications. [17–22] Gels are formed by the self-assembly of molecules in solution into a network of fibrous structures. As the self-assembly is driven by non-covalent interactions, such gels show excellent responsiveness towards various physical and chemical stimuli such as temperature, light, and pH amongst others and are extensively used for biomimicry. In the last decade, there has been an enormous development in synthesizing self-assembled systems inspired by biology using such gels (Fig. 1a). [23–26] Typically, these dynamic systems show a sol-gel phase transformation in presence of an energy input, which can often be reversed by the addition of a counter input. Limited attempts have been made to explore mini-homeostatic modules in designing of autonomous materials involving supramolecular gels where the systems maintain their form throughout the energy cycle (Fig. 1b). For example, He et al. demonstrated a hydrogel-supported bilayer system that exhibits chemo-mechano-chemical self-regulation and utilized the platform to perform several exothermic catalytic reactions. [10] Most of the examples found in this domain concentrate on the application or outcome of such systems, however how these mini-homeostatic modules evolve under the influence of a feedback loop is still unexplored. [6, 10, 27, 28] The effect of a reaction cycle on the synthetic homeostatic system also needs to be addressed.

In this work, we devise a strategy to construct a hydrogel-based homeostatic system and investigate the microscopic and macroscopic changes in presence of a chemical reaction cycle (Fig. 1c). The on-off switching of the reaction cycle results in different feedback from the gel and creates three mini-homeostatic modules with time. We investigate the temporal evolution of the mini-homeostatic modules and determine the influence of kinetics on the properties of our homeostatic system.

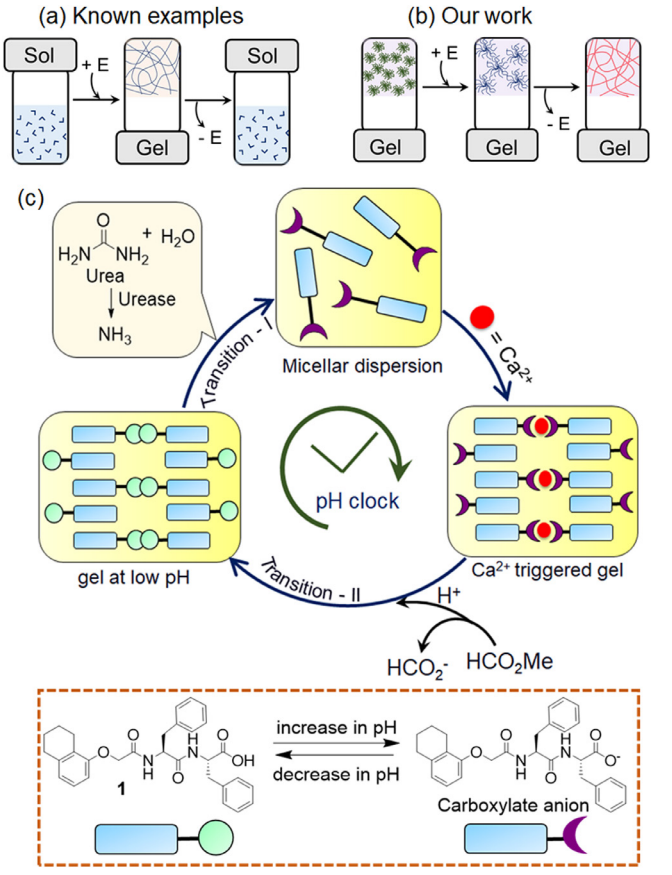

Fig. 1

(a-b) Schematic representation showing the difference of our system with the reported systems consisting an energy (E) cycle. (c) Cartoon representing the temporal evolution of a homeostatic hydrogel system formed from **1** and Ca^{2+}. At high pH, the system maintains its gel structure by coordinating to Ca^{2+} ions. In the presence of a feedback loop, the hydrogel evolves through a gel-to-gel-to-gel transition creating three mini-homeostatic modules (representing each gel state) over time.

Results and discussion

We use dipeptide **1** to construct the basic platform of our homeostatic system. As we have described previously, **1** forms a gel almost instantly in DMSO/H_2O (20/80, v/v) at a concentration of 2 mg/mL with a pH of around 4.3 (Fig. S1). [29] Oscillatory rheology experiments confirm the viscoelastic nature of the gel that arises from a network of spherulitic domains of fibers as shown by confocal microscopy imaging (Figure S1). [29] Such gels are pH responsive; increasing the pH above the apparent pK_a of **1** (~6.4, Figure S2) results in formation of a micellar dispersion, and so a gel-to-sol phase transition. [29, 30]

We coupled this system with a pH cycle to generate feedback loops through a responsive and restorative function which is an essential criterion for a homeostatic system to work. [6] To construct the pH cycle, we used a previously reported method, coupling the urease-urea reaction (a fast activator) with hydrolysis of methyl formate (a dormant deactivator). [25, 29] The urease catalyzed hydrolysis of urea produces NH_3 as base and results in an increase in the pH. [31–33] There was no considerable change in the activity of the enzyme was observed in DMSO/water (20/80 v/v) compared to normal water (Figure S2). Only a slight reduction in the rate of pH change for initial 10 seconds was noticed in DMSO-water. For the hydrogel system, at a pH above the apparent pK_a of **1**, deprotonation of the carboxylic acid causes disassembly of the gel network, resulting in a return to the solution state (Fig. 2a and b). At high pH, the hydrolysis of methyl formate is accelerated and the production of formic acid results in a reduction in pH of the medium, which causes reassembly and re-gelation (Fig. 2b and Figure S3). [29] The physical behaviour of the gel correlates with the changes in pH and a visual transformation of the initially formed gel to a free-flowing solution followed by

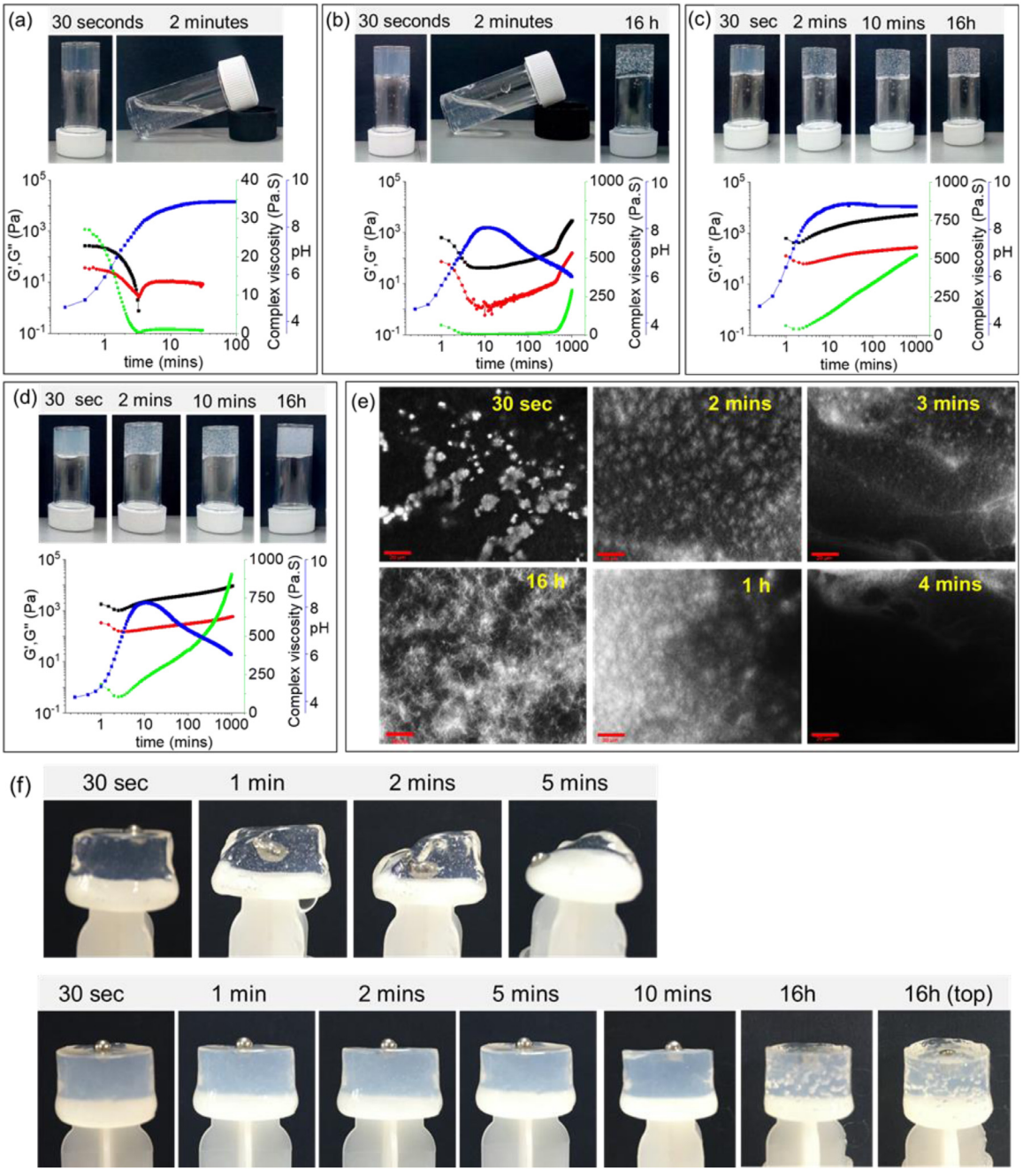

Fig. 2

(a)-(d) Variation of pH (blue), G′ (black), G″ (red) and complex viscosity (green) with time for **1** in presence of urea-urease reaction under different initial conditions. The enzymatic reaction is performed (a) in absence of both methyl formate and Ca^{2+}; (b) in presence of methyl formate but in absence of Ca^{2+}; (c) in presence of Ca^{2+} but in absence of methyl formate; (d) in presence of both methyl formate and Ca^{2+}. For (a)-(d), the photographs represent phase changes of **1** with time associated to the respective chemical reactions. The structures in the gel are air bubbles, not precipitation. (e) Time dependent confocal microscopy images of **1** involving urea-urease reaction under conditions applied for (d). Scale bars represent 20 μm. In all cases, solvent is 20/80 DMSO/water (v/v) and [**1**] = 2 mg/mL. Initial [urease] = 0.2 mg/mL, [urea] = 0.02 M, volume of methyl formate = 100 μL and [Ca^{2+}] = 0.5 equiv. (used as required). (f) Photographs of (top) the system with no Ca^{2+} and (bottom) with Ca^{2+}. Gels were prepared in a mould and quickly removed. A ball bearing was placed on top of the gel immediately after removal from the mould. In the absence of the Ca^{2+}, the gel-to-sol transition mean the liquid flows away and hence no photographs are shown after 5 minutes. The data shown in Fig. 2a and 2b have been redrawn from reference 29.

re-gelling was observed over time. Hence, coupling of a chemical reaction and a hydrolysis agent induces a pH-regulated gel-to-sol-to-gel phase transition. Hence, the gel loses its integrity at high pH. For the system to function as a homeostatic module, instead of a gel-to-sol-to-gel transition, it needs to evolve through a gel-to-gel-to-gel transition.

To achieve this gel-to-gel-to-gel transition, cross-linking of the micellar dispersion of **1** at high pH is possible using divalent

cations. [30] When incorporating Ca^{2+} ions, into the system, the production of NH_3 by the enzyme again results in the pH increasing rapidly and reaching a plateau at pH 9.0-9.1 after ~1 hour (Fig. 2c). The initially turbid gel became transparent without any obvious phase transformation to a solution state. To investigate the effect of Ca^{2+} on gelation kinetics, time sweep rheology as well as viscosity data were recorded in absence and presence of Ca^{2+} (Fig. 2a and Fig. 2c). There were slight differences in the rate of pH increase, but the main differences can be seen from the rheological data. Without Ca^{2+}, both the storage (G′) and loss (G″) modulus of the gel decreased as the pH increases, with G′ being less than G″ above the apparent pK_a of **1**. In comparison, in the presence of Ca^{2+}, both G′ and G″ started to increase slowly after 2 minutes. Viscosity data recorded over time in absence and presence of Ca^{2+} follow similar trends as that of rheology. The Ca^{2+}-triggered system showed significantly higher values of both viscosity and the rheological moduli at high pH, supporting the visual observations that a gel is formed. Hence, the Ca^{2+} ions prevent sol formation and result in a gel-to-gel transition (Fig. 2c and Fig. S4). This can be clearly shown comparing systems that have been removed from a mould (Fig. 2f).

We recorded the variation of pH with time for **1** in presence of Ca^{2+} involving the pH cycle (Fig. 1 and 2d). There was a slight drop in the initial pH value compared to the case when Ca^{2+} is absent (Fig. 2b, Fig. 2d and Fig. S5). This induced a negative feedback on the rate of pH increase at the early stages although no change either in the maximum pH or in the rate of pH decrease was found. In the absence of Ca^{2+}, both G′ and G″ started to decrease and reached minima after 6 minutes (Fig. 2b). In presence of Ca^{2+}, after a slow initial decrease, both G′ and G″ started to increase after 2 minutes confirming reconstruction of a new type of network involving the Ca^{2+} ions with no formation of a solution phase (Fig. 2d). Moreover, at high pH, the system exhibits higher values of both the viscosity and the rheological moduli (>25 times), suggesting binding of the Ca^{2+} ions to the micellar aggregates of **1**. Interestingly, after ~6 hours, when the pH again decreases to the apparent pK_a of **1**, the rheological moduli showed a slight increase in magnitude due to a transition from a salt-driven state to the pH-driven state. Such a transition was not observed when Ca^{2+} was present alone (Fig. 2c). Moreover, such a pH driven transition after ~6 hours was more prominent when Ca^{2+} was absent (Fig. 2b). Comparison of the results from Fig. 2b and Fig. 2d suggests that the presence of Ca^{2+} ions results in the system resisting the structural deformations and phase transformation of the system throughout the pH cycle; during the experiment, no sol formation was noticed. Hence, our hydrogel system exhibits homeostasis in presence of Ca^{2+} and a pH cycle showing a gel-to-gel-to-gel transition where each gel state represents an individual mini-homeostatic module. The self-monitoring properties of individual mini-homeostatic modules arise from the choice of whether or not to bind the Ca^{2+} depending on the pH of the medium. There may not be a specific time at which one type of gel transforms to another; the gelation is either pH triggered or Ca^{2+}-triggered and this depends on the protonation state of the terminal carboxylic acid. As such, it is likely that there is a time period where the system is at a pH around the pK_a of **1** where both triggers are causing gelation of at least some of the system. Interestingly, the final values of both rheological moduli and the viscosity were considerably higher than for the initially formed gel. Homeostasis allows the system to evolve into a more homogeneous structure and enable to self-correct the errors being present in the initially formed kinetically trapped gel. Hence, the evolution of the mini-homeostatic modules induces self-monitoring and self-regulating behaviour on our system leading to improvement in the mechanical properties in terms of both gel stiffness and gel strength (Fig. 2d, Fig. S6 and Table S1). Other groups have reported self-regulated gel-to-gel transitions; [34–37] however, three stages of gel evolution are unknown in the literature.

To understand the development of the microstructure underlying the gel at each point during the evolution, confocal microscopy imaging was conducted at different time intervals. At early times, spherulitic domains of fibers were imaged as expected for gels by a solvent-triggered approach (Fig. 2e). As the pH of the medium increases with time, the density of the spherical aggregates decreases and a new type of densely packed spherulitic aggregate appeared. These spherulitic domains of fibers are very similar to those are formed at high pH in presence of Ca^{2+} alone (Fig. 2c and Fig. S7). At longer times as the pH decreases once again, the system further evolves to a long fibrous network. In comparison to the original gel, the gel obtained after the pH cycle contains fewer spherulitic domains and instead a higher density of long fibres (Fig. 2e and Fig. S8). Hence, the differences in the final rheological properties can be correlated to changes in the underlying network.

It is possible to control the evolution of each of the mini-homeostatic modules by controlling the growth and development of individual gel states including the lifetime, mechanical properties, and microstructure of the gels. To do this, we gradually increased the concentration of methyl formate, whilst keeping all other parameters fixed. Increasing the concentration of methyl formate causes a substantial reduction in the rate of pH increase as well as the maximum pH. The maximum pH of the reaction medium reduced from pH 8.2 (using 100 μL of methyl formate) to pH 7.7 (using 200 μL) (Fig. 3a). There was also a drop in the final pH of the medium from pH 6.0 (using 100 μL of methyl formate) to pH 5.2 (using 200 μL). The differences in the pH-time profile results in different stability and mechanical properties of individual gel states (or mini-homeostatic modules). The change in the kinetics of the change in pH over the course of the experiment directly translates into delay in the decrease of both G′ and G″, and thereby emphasizes an increase in the lifetime of the primary assembled structures (from around 2 minutes to around 4 minutes) although no significant change in the absolute stiffness (G′) or the complex viscosity values of the primary gel states was found (Fig. 3a and 3b). These changes also correlate with changes in the time variable UV-vis data, where the decrease in absorbance at 380 nm is progressively delayed with the decrease in the rate of pH increase (Fig. S10). In the transient, high pH regime, the absolute stiffness (G′) and the complex viscosity values of the Ca^{2+}-triggered gel state notably decreased (by around 30%). However, no substantial change in the gel lifetime was observed from rheological studies (Fig. 3a and Fig. 3b). Interestingly, the

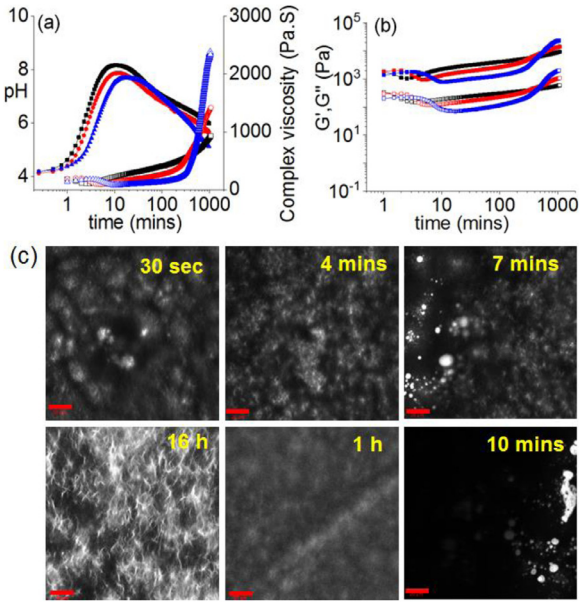

Fig. 3

(a) Variation of pH (close symbol) and complex viscosity (open symbol), and (b) Variation of G′ (close symbol) and G″ (open symbols) with time for **1** from the enzymatic reaction in presence methyl formate and Ca^{2+}. In both cases, volume of methyl formate used is 100 μL (black), 150 μL (red) and 200 μL (blue). (c) Time dependent confocal microscopy images of **1** involving urea-urease reaction in presence of 200 μL of methyl formate and Ca^{2+}. Scale bars represent 20 μm. In all cases, initial condition is: [urease] = 0.2 mg/mL, [urea] = 0.02 M, and [Ca^{2+}] = 0.5 equiv. Solvent is 20/80 DMSO/water (v/v) and [**1**] = 2 mg/mL.

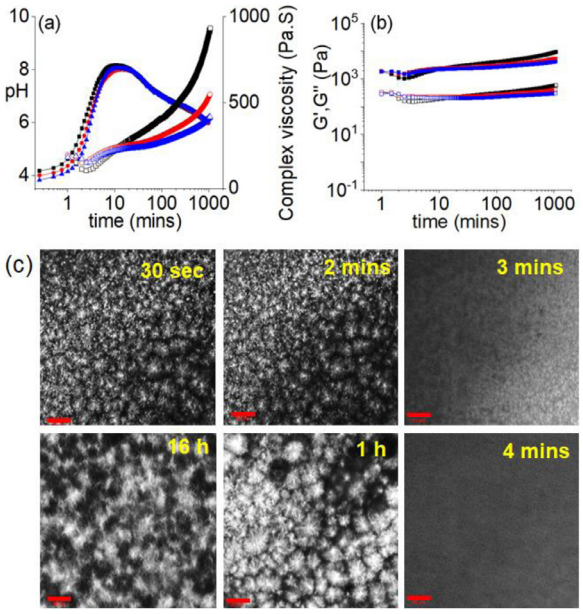

Fig. 4

(a) Variation of pH (closed symbol) and complex viscosity (open symbol), and (b) variation of G′ (close symbol) and G″ (open symbols) with time for **1** from the enzymatic reaction in presence methyl formate and Ca^{2+}. In both cases, [Ca^{2+}] is 0.5 equiv. (black), 1.0 equiv. (red) and 2.0 equiv. (blue). (c) Time dependent confocal microscopy images of **1** involving urea-urease reaction in presence of methyl formate and 2 equiv. of Ca^{2+}. Scale bars represent 20 μm. In all cases, initial condition is: [urease] = 0.2 mg/mL, [urea] = 0.02 M, and volume of methyl formate is 100 μL. Solvent is 20/80 DMSO/water (v/v) and [**1**] = 2 mg/mL.

viscosity and rheological moduli of the final gels increases with the reduction in the final pH values. Again, at high pH, the Ca^{2+}-triggered gels result in formation of different spherulitic arrangement of fibres as compared to the initially formed material. Interestingly, with a gradual decrease in the pH of the final gels, the density of the spherulitic domains decreases with a dominance of long fibres (Fig. S11). The higher density of long fibres correlates with a higher stiffness (G′) of the materials (Fig. S12 and Table S2). These gels also show a gradual decrease in the strain bearing capacity (the critical strain) of the final gels (Fig. S12). We suggest that networks consisting of spherulitic domains can withstand a higher strain compared to the long fibres.

The properties of the mini-homeostatic gels can also be controlled by adjusting the concentration of Ca^{2+} ions (keeping all other parameters fixed). An increase in Ca^{2+} ion concentration only extends the negative feedback on pH-time profile, while imposing no major change either in the maximum pH or in the rate of pH decrease (Fig. 4a). There was also no significant change in the final pH values. By rheology, no substantial change in the lifetime of either the initially assembled structures or the Ca^{2+}-bound structures was observed (Fig. 4a, 4b). However, the absolute stiffness (G′) as well as the viscosity values of the final gels decreased with an increase in the initial concentration of Ca^{2+} (Fig. 4b). These results suggest that an increase in the Ca^{2+} ion concentration leads to a structure at high pH that prevents the system to evaluate easily. This was clearly reflected by UV-Vis spectroscopy and confocal studies. By UV-Vis spectroscopy, the changes in absorbance at 380 nm is restricted for the systems containing a higher concentration of Ca^{2+} ions (Fig. S13). These variations arise from the difference in underlying molecular packing in the gels formed in respective time scales (Fig. 2e and Fig. 4c). Increasing the concentration of Ca^{2+} ions results in the formation of a higher density of large spherulitic domains of fibres both at the beginning of the pH cycle as well as in the high pH state. The reason for change in aggregated structures with increasing concentration of Ca^{2+} ions can be ascribed to the salt affecting the structuring of the peptide network involving the Hofmeister effect. Dissolving a salt in water have a significant effect on water structure and dynamics [38] which leads to the differences in hydration of the peptide. [39] As consequence, there is a change in the nucleation centre followed by the growth of nanostructures. [40] When the Ca^{2+}-triggered gels finally evolves to the pH-triggered gels, the systems having a higher concentration of Ca^{2+} ions display a higher density of spherulitic domains and fewer long fibres (Fig. 4c, S14). Consequently, the final material shows a ~40% reduction in stiffness of the gel accompanying with ~60% increase in gel strength (critical strain) (Fig. S15 and Table S3). These results suggest that there is always a tussle inside the system induced by Ca^{2+} ions throughout the pH cycle that apparently try to resist the structural deformations. The results further emphasize that pH is not the only determining factor of the properties of the individual mini-homeostatic gel states, Ca^{2+} ions too play a decisive role on

the stability, microstructure as well as mechanical properties of the states during evolution.

It is further possible to probe the evolution of the gel by adjusting the urease and urea concentration (keeping all other parameters fixed). Either a decrease in urea or urease concentration results in a reduction in the production of NH_3 and thereby decrease the rate of initial pH increase (Fig. S16). A 50% reduction in enzyme concentration delays the transition of the initially formed gel (the lifetime increases from ~2 mins to ~5 mins) to the Ca^{2+}-triggered gel (Fig. S16). However, no major difference in the pH decay profile as well as in the final pH was observed. Although the pH-time profiles are dependent on initial reaction conditions, the viscosities and rheological moduli the respective mini-homeostatic modules during the evolution process under different conditions are very similar (for example after 1 minute, 1 hour and 16 hours). The microstructure and the mechanical properties of the final gels were also similar (Fig. S17 and S18, Table S4).

An interesting question is whether the system can show homeostatic property on performing more pH-cycles after the first gel-gel-gel transition. For our system, the pH change is driven by two consecutive chemical reactions; production of NH_3 from the urea-urease reaction followed by alkaline hydrolysis of methyl formate. As we are form a gel throughout the cycle, the final state is still a gel. As such, it is hard to perform repetitive operations involving such chemical reaction driven pH-cycle through post assembly fabrication method because of the issues related to the mixing of the components. After the first cycle, further addition of urea and methyl formate resulted in a slight increase in pH (from pH 6.0 to 6.7) followed by return to the initial pH state (pH 5.9) (Fig. S19). As expected, the gel state is maintained throughout the second pH cycle. On the other hand, when we exposed the final gel to a vapour of ammonia, the gel state persists, and the pH increased to 10.5 (Figure S20). On further treatment with methyl formate, the system did not revert to the low pH state. Hence, post-assembly fabrication is not suitable to perform repetitive pH cycles.

In conclusion, we have successfully mimicked the evolution of mini-homeostatic modules by creating a homeostatic hydrogel system. Typically, the concept of homeostasis refers to a dynamic system which is always ready to reset itself for survival in response to a change in the environment. [41] In this work, we tried to mimic a concept by which a gel system can sustain its gel structure during evolution in presence of a feedback loop. We consider the maintenance of phase integrity throughout an energy cycle as the essential criterion of homeostasis. Our homeostatic system shows self-regulating and self-monitoring properties and evolves through a gel-to-gel-to-gel transition by creating three mini-homeostatic modules in one cycle. We can tune the lifetime of the transitions as well as properties of the individual mini-homeostatic modules by controlling the initial energy input provided to the system. During the evolution, the properties of the individual mini-homeostatic modules not only depend on the rate of activation and deactivation kinetics of the pH cycle but also on the Ca^{2+} ion concentration, where responsiveness of the precursor towards the environment is the key factor to determine the lifetime as well as the mechanical properties of the mini-homeostatic modules. Importantly, control over the evolution of the mini-homeostatic modules induces the self-correcting opportunity to our homeostatic hydrogel system through which we can tune the network type and improve the mechanical properties of the homeostatic gel system. Unlike other dynamic gels that loses its phase integrity while working under feedback loops, [23–26] our system maintains its gel form (i.e exhibits homeostasis) throughout the energy cycle. We envisage that maintaining phase behaviour during dynamic evolution is a new concept and can be applied to synthesize next generation functional materials.

Methods

Materials: Compound **1** was synthesised as described previously (Fig. S21, S22). [42] Urease (J61455 Urease, Jack Beans, minimum 45.0 units/mg solid) and urea (ultrapure 99%) were obtained from Alfa Aesar. Methyl formate was purchsed from Sigma Aldrich. $CaCl_2$ (granular) was obtained from Fisher Scientific. Deionised water was used throughout all experiments.

Preparation of solutions: A stock solution of **1** was prepared in DMSO at a concentration of 10 mg/mL. The enzyme, urea and $CaCl_2$ were highly soluble in H_2O and therefore did not require stirring. The stock solutions of the enzyme was prepared at concentrations of 0.254 mg/mL and 0.127 mg/mL in H_2O. The enzyme concentration in the stock solution was determined from the mass (in mg) dissolved in known volume of H_2O. Stock solutions of the urea and $CaCl_2$ were prepared in H_2O in the concentration of 2 M and 1 M, respectively. Solutions of urease, urea and $CaCl_2$ were prepared freshly before each experiment. Molar equivalents of Ca^{2+} were calculated with respect to the molar concentration of **1**.

The enzyme-catalyzed reactions involving gelator **1** were performed either in presence and absence of methyl formate and Ca^{2+} or both. For the enzymatic reactions in absence of both methyl formate and Ca^{2+}, 1.580 mL of the urease solution of concentration 0.254 mg/mL was transferred to the vial containing 0.40 mL of the gelator solution and urea (20 μL in H_2O) and left undisturbed. Therefore, the final ratio of DMSO and H_2O was 20:80, the concentration of **1** was 2 mg/mL, the concentration of urease was 0.2 mg/mL and the initial concentration of urea was 0.02 M. A similar method was used to perform the enzymatic reactions in presence of Methyl formate. In this case, urease solution was added to the mixture of **1**, urea and methyl formate (100 μL) and the same solutions of **1**, urease and urea in respected volumes were used as above. Similarly, for the enzymatic reactions in presence of Ca^{2+}, urease solution was added to the mixture of **1**, urea and $CaCl_2$ (4 μL) and the same solutions of **1**, urease and urea in respected volumes were used as above.

For the enzymatic reactions in presence of both methyl formate and Ca^{2+}, 1.580 mL of the urease solution (0.254 mg/mL or 0.127 mg/mL as required) was added to the vial containing 0.40 mL of the gelator solution, urea (20 μL of urea or a mixture of 10 μL of urea and 10 μL of H_2O, as required), $CaCl_2$ (4 μL, 8 μL or 16 μL as required) and methyl formate (100 μL, 150 μL or 200 μL as required). Throughout these experiments a total solvent volume of ~2 mL was maintained in which the final ratio of DMSO and H_2O was 20:80. Therefore, the concentration of **1** was 2 mg/mL,

the concentration of urease was 0.2 mg/mL and 0.1 mg/mL as required, the concentration of Ca^{2+} was 0.5, 1 and 2 equiv. as required, and the initial concentration of urea was 0.02 M and 0.01 M as required. In all cases, molar equivalents of Ca^{2+} were calculated with respect to the molar concentration of **1**.

Hydrogel Formation: Hydrogels of **1** were prepared under different conditions. For the solvent switch method, 1.6 mL of water was added to 0.4 mL of the DMSO solution of **1** to form the hydrogel. The hydrogel of **1** was also prepared in presence of urease (0.2 mg/mL) by replacing water with auqeous solution of urease. To prepare the gel in presence of both urease (0.2 mg/mL) and Ca^{2+} (0.5 equiv.), aqueaous solution of urease was added to the mixture of **1** and Ca^{2+}. The final gelator concentration was 2 mg/mL. The samples were left overnight before measurements were carried.

For the Ca^{2+}-triggered gels at high pH, the gelation experiments were carried out by adding urease solutions to the mixture of **1**, urea and Ca^{2+} as mentioned above. The samples were then left to stand overnight to allow gelation.

Gels were also prepared involving the urease-urea reaction in presence of both Ca^{2+} and methyl formate. To prepare these gels, aqueous solutions of urease was added to the mixture of **1**, urea, methyl formate and $CaCl_2$ in their respected volumes as mentioned above.

In all cases, a total solvent volume of ~2 mL was maintained in which the final ratio of DMSO and H_2O was 20:80. The gelator oncentration was 2 mg/mL. For all Ca^{2+}-gels, the molar equivalents of Ca^{2+} were calculated with respect to the molar concentration of **1**.

pH measurements: A FC200 pH probe from HANNA instruments with a 6 mm x 10 mm conical tip was used for pH measurements. The stated accuracy of the pH measurements is ±0.1. For the urea-urease reaction involving the gelator, the reaction mixtures were prepared as described above at a 2 mL volume in a 7 mL Sterilin vial and the pH change was monitored with time. The temperature was maintained at 25°C during the measurement by using a circulating water bath. pK_a determination was carried out by recording the pH values after each addition of HCl (0.1M) to the solution of **1** (concentration is 2 mg/mL) containing 1 molar equivalents of NaOH (0.1 M) in 20% DMSO in H_2O. During the titration, to prevent any gel formation, the solution was stirred continuously. The experimental temperature was 25 °C.

Rheological and viscosity measurements: All rheological measurements were undertaken on an Anton Paar Physica MCR 301 rheometer at 25 °C. Strain, frequency, temperature and time sweeps were performed using a vane and cup geometry. Strain sweeps were performed at 10 rad/s from 0.01 % to 1000 % strain. Frequency sweeps were carried out from 1 rad/s to 100 rad/s at 0.5 % strain. All gels were left ~16 hours before being measured. Time sweeps were performed at an angular frequency of 10 rad/s and with a strain of 0.5%. For all experiments, gels were prepared as mentioned earlier in 2 mL volume in a 7 mL Sterilin vials.

Confocal microscopy: A Zeiss LSM710 confocal microscope (Zeiss, Gottingen, Germany) with an LD EC Epiplan NEUFLUAR 50X, 0.55 DIC (Carl Zeiss, White Plains, NY, USA) objective was used for imaging. Samples were prepared as mentioned earlier containing Nile blue (2 μL/mL of a 0.1 wt % solution) in CELLview Culture dishes (35 mm diameter) and were excited at 633 nm using a He-Ne laser. Images were captured using the software Carl Zeiss ZEN 2011 v7.0.3.286.

UV-Vis measurements: Data were collected on an Agilent Cary 60 UV-vis spectrophotometer. All UV-vis experiments were carried out in presence of 20 μL of 0.005 M pyrene (in DMSO). Samples were prepared in a PMMA cuvette with a path length of 1 cm by following the same procedure as mentioned before.

Declaration of Competing Interest

The authors declare that they have no known competing financial interests or personal relationships that could have appeared to influence the work reported in this paper.

Acknowledgements

SP thanks the University of Glasgow for funding. DA thanks the EPSRC for a Fellowship (EP/L021978/2).

Supplementary materials

Supplementary material associated with this article can be found, in the online version, at doi:10.1016/j.giant.2020.100041.

References

[1] B. Hatton, L. Mishchenko, S. Davis, K.H. Sandhage, J. Aizenberg, Assembly of large-area, highly ordered, crack-free inverse opal films, Proc. Natl. Acad. Sci. 107 (23) (2010) 10354–10359, doi:10.1073/pnas.1000954107.

[2] G. Bao, R.D. Kamm, W. Thomas, W. Hwang, D.A. Fletcher, A.J. Grodzinsky, C. Zhu, M.R.K. Mofrad, Molecular biomechanics: the molecular basis of how forces regulate cellular function, Cel. Mol. Bioeng. 3 (2) (2010) 91–105, doi:10.1007/s12195-010-0109-z.

[3] D.J. Kushner, Self-assembly of biological structures, Bacteriol Rev. 33 (2) (1969) 302–345.

[4] G.M. Whitesides, B. Grzybowski, Self-Assembly at All Scales, Science 295 (5564) (2002) 2418–2421 http://science.sciencemag.org/content/295/5564/2418.

[5] J.H. van Esch, R. Klajn, S. Otto, Chemical systems out of equilibrium, Chem. Soc. Rev. 46 (18) (2017) 5474–5475, doi:10.1039/C7CS90088K.

[6] M.M. Lerch, A. Grinthal, J. Aizenberg, Viewpoint: homeostasis as inspiration—toward interactive materials, Adv. Mater. 32 (20) (2020) 1905554, doi:10.1002/adma.201905554.

[7] B.A. Grzybowski, W.T.S. Huck, The nanotechnology of life-inspired systems, Nat. Nanotechnol. 11 (7) (2016) 585–592, doi:10.1038/nnano.2016.116.

[8] H. Hess, J.L. Ross, Non-equilibrium assembly of microtubules: from molecules to autonomous chemical robots, Chem. Soc. Rev. 46 (18) (2017) 5570–5587, doi:10.1039/C7CS00030H.

[9] P. Fratzl, F.G. Barth, Biomaterial systems for mechanosensing and actuation, Nature 462 (7272) (2009) 442–448, doi:10.1038/nature08603.

[10] X. He, M. Aizenberg, O. Kuksenok, L.D. Zarzar, A. Shastri, A.C. Balazs, J. Aizenberg, Synthetic homeostatic materials with chemo-mechano-chemical self-regulation, Nature 487 (7406) (2012) 214–218, doi:10.1038/nature11223.

[11] D. Stamenović, M.L. Smith, Tensional homeostasis at different length scales, Soft Matter 16 (30) (2020) 6946–6963, doi:10.1039/D0SM00763C.

[12] A. Takeda, M. Nakamura, H. Fujii, H. Tamano, Synaptic Zn2+ homeostasis and its significance, Metallomics 5 (5) (2013) 417–423, doi:10.1039/C3MT20269K.

[13] A. Bhattacharjee, K. Chakraborty, A. Shukla, Cellular copper homeostasis: current concepts on its interplay with glutathione homeostasis and its implication in physiology and human diseases, Metallomics 9 (10) (2017) 1376–1388, doi:10.1039/C7MT00066A.

[14] A.K. Mandal, D.B. Mount, The molecular physiology of uric acid homeostasis, Annu. Rev. Physiol. 77 (1) (2015) 323–345, doi:10.1146/annurev-physiol-021113-170343.

[15] E. Laskowska, D. Kuczyńska-Wiśnik, B. Lipińska, Proteomic analysis of protein homeostasis and aggregation, J. Proteomics 198 (2019) 98–112, doi:10.1016/j.jprot.2018.12.003.

[16] W.B. Cannon, Organization for physiological homeostasis, Physiol. Rev. 9 (3) (1929) 399–431, doi:10.1152/physrev.1929.9.3.399.

[17] C. Echeverria, S.N. Fernandes, M.H. Godinho, J.P. Borges, P.I.P. Soares, Functional stimuli-responsive gels: hydrogels and microgels, Gels 4 (2) (2018) 54, doi:10.3390/gels4020054.

[18] J. Hoque, N. Sangaj, S. Varghese, Stimuli-responsive supramolecular hydrogels and their applications in regenerative medicine, Macromol. Biosci. 19 (1) (2019) 1800259, doi:10.1002/mabi.201800259.

[19] Z. Deng, H. Wang, P.X. Ma, B. Guo, Self-healing conductive hydrogels: preparation, properties and applications, Nanoscale 12 (3) (2020) 1224–1246, doi:10.1039/C9NR09283H.

[20] J. Li, W.-Y. Wong, X.-m. Tao, Recent advances in soft functional materials: preparation, functions and applications, Nanoscale 12 (3) (2020) 1281–1306, doi:10.1039/C9NR07035D.

[21] J. Li, L. Geng, G. Wang, H. Chu, H. Wei, Self-healable gels for use in wearable devices, Chem. Mater. 29 (21) (2017) 8932–8952, doi:10.1021/acs.chemmater.7b02895.

[22] Y. Wang, W. Zhang, C. Gong, B. Liu, Y. Li, L. Wang, Z. Su, G. Wei, Recent advances in the fabrication, functionalization, and bioapplications of peptide hydrogels, Soft Matter 16 (44) (2020) 10029–10045, doi:10.1039/D0SM00966K.

[23] B. Rieß, R.K. Grötsch, J. Boekhoven, The design of dissipative molecular assemblies driven by chemical reaction cycles, Chem 6 (3) (2020) 552–578, doi:10.1016/j.chempr.2019.11.008.

[24] G. Wang, S. Liu, Strategies to construct a chemical-fuel-driven self-assembly, ChemSystemsChem 2 (4) (2020) e1900046, doi:10.1002/syst.201900046.

[25] S. Panja, C. Patterson, D.J. Adams, Temporally-programmed transient supramolecular gels, Macromol. Rapid Commun. 40 (15) (2019) 1900251, doi:10.1002/marc.201900251.

[26] N. Singh, G.J.M. Formon, S. De Piccoli, T.M. Hermans, Devising synthetic reaction cycles for dissipative nonequilibrium self-assembly, Adv. Mater. 32 (20) (2020) 1906834, doi:10.1002/adma.201906834.

[27] L.D. Zarzar, J. Aizenberg, Stimuli-responsive chemomechanical actuation: a hybrid materials approach, Acc. Chem. Res. 47 (2) (2014) 530–539, doi:10.1021/ar4001923.

[28] C. Zheng, Q. Zeng, S. Pimpi, W. Wu, K. Han, K. Dong, T. Lu, Research status and development potential of composite hemostatic materials, J. Mater. Chem. B 8 (25) (2020) 5395–5410, doi:10.1039/D0TB00906G.

[29] S. Panja, A.M. Fuentes-Caparrós, E.R. Cross, L. Cavalcanti, D.J. Adams, Annealing supramolecular gels by a reaction relay, Chem. Mater. 32 (12) (2020) 5264–5271, doi:10.1021/acs.chemmater.0c01483.

[30] L. Chen, G. Pont, K. Morris, G. Lotze, A. Squires, L.C. Serpell, D.J. Adams, Salt-induced hydrogelation of functionalised-dipeptides at high pH, Chem. Commun. 47 (44) (2011) 12071–12073, doi:10.1039/C1CC15474E.

[31] G. Hu, J.A. Pojman, S.K. Scott, M.M. Wrobel, A.F. Taylor, Base-catalyzed feedback in the urea–urease reaction, J. Phys. Chem. B 114 (44) (2010) 14059–14063, doi:10.1021/jp106532d.

[32] T. Heuser, E. Weyandt, A. Walther, Biocatalytic feedback-driven temporal programming of self-regulating peptide hydrogels, Angew. Chem. Int. Ed. 54 (45) (2015) 13258–13262, doi:10.1002/anie.201505013.

[33] H.E. Cingil, N.C.H. Meertens, I.K. Voets, Temporally programmed disassembly and reassembly of C3Ms, Small 14 (46) (2018) 1802089, doi:10.1002/smll.201802089.

[34] Y. Zhong, P. Li, J. Hao, X. Wang, Bioinspired self-healing of kinetically inert hydrogels mediated by chemical nutrient supply, ACS Appl. Mater. Interfaces 12 (5) (2020) 6471–6478, doi:10.1021/acsami.9b20445.

[35] E.R. Draper, T.O. McDonald, D.J. Adams, Photodimerisation of a coumarin-dipeptide gelator, Chem. Commun. 51 (64) (2015) 12827–12830, doi:10.1039/C5CC03817K.

[36] S.J. Beckers, S. Parkinson, E. Wheeldon, D.K. Smith, In situ aldehyde-modification of self-assembled acyl hydrazide hydrogels and dynamic component selection from complex aldehyde mixtures, Chem. Commun. 55 (13) (2019) 1947–1950, doi:10.1039/C8CC09395D.

[37] C. Mahendar, M.K. Dixit, Y. Kumar, M. Dubey, d-(+)-Glucose-triggered metallogel to metallogel transition, J. Mater. Chem. C 8 (32) (2020) 11008–11012, doi:10.1039/D0TC02877K.

[38] B. Hribar, N.T. Southall, V. Vlachy, K.A. Dill, How ions affect the structure of water, J. Am. Chem. Soc. 124 (41) (2002) 12302–12311, doi:10.1021/ja026014h.

[39] A.Z. Cardoso, L.L.E. Mears, B.N. Cattoz, P.C. Griffiths, R. Schweins, D.J. Adams, Linking micellar structures to hydrogelation for salt-triggered dipeptide gelators, Soft Matter 12 (15) (2016) 3612–3621, doi:10.1039/C5SM03072B.

[40] S. Roy, N. Javid, J. Sefcik, P.J. Halling, R.V. Ulijn, Salt-induced control of supramolecular order in biocatalytic hydrogelation, Langmuir 28 (48) (2012) 16664–16670, doi:10.1021/la303388s.

[41] J.S. Torday, Homeostasis as the mechanism of evolution, Biology 4 (3) (2015) 573–590, doi:10.3390/biology4030573.

[42] M.C. Nolan, A.M. Fuentes Caparrós, B. Dietrich, M. Barrow, E.R. Cross, M. Bleuel, S.M. King, D.J. Adams, Optimising low molecular weight hydrogels for automated 3D printing, Soft Matter 13 (45) (2017) 8426–8432, doi:10.1039/C7SM01694H.